Supporting Information

Synchronizing O_2 Adsorption and Proton-Coupled Electron Transfer in Carboxylated Quinoline-Linked Covalent Organic Frameworks to Boost Photocatalytic H_2O_2 Production

Hao Wang,[a] Junjiang Zong,[a] Shiyuan Wei,[a] Meng Li,[a] Xiaodong Sun,[c] Liqun Ye,[d] Jianhan Huang,*[a] Jiawei Li,*[a] You-Nian Liu [a] and Tianyi Ma[b]

[a] College of Chemistry and Chemical Engineering, Key Laboratory of Micro and Nano Material Interface Science, Central South University, Changsha, 410083, China

[b] School of Science, Centre for Atomaterials and Nanomanufacturing (CAN), RMIT University, Melbourne, VIC 3000, Australia

[c] Institute of Clean Energy Chemistry, Key Laboratory for Green Synthesis and Preparative Chemistry of Advanced Materials, College of Chemistry, Liaoning University, Shenyang, 110036, China

[d] College of Materials and Chemical Engineering, Key Laboratory of inorganic nonmetallic crystalline and energy conversion materials, China Three Gorges University, Yichang, 443002, China

1. Materials and Methods

1.1 Materials

4,4',4"-(1,3,5-Triazine-2,4,6-triyl)trianiline (TAPT) (CatNo.1062431, Leyan, Shanghai, China), 5,5′,5″-(1,3,5-Benzenetriyl)tris[2-pyridinecarboxaldehyde] (BTPA), ammonium iodide, di-tert-butyl peroxide, triethylamine, pyruvic acid, 1,4-dioxane, mesitylene, acetic acid (HAc), nitrotetrazolium blue chloride (NBT) (CatNo.1079584, Leyan, Shanghai, China), acetone, potassium iodide (KI), potassium bromate ($KBrO_3$), ammonium oxalate and p-benzoquinone (pBQ) were purchased from Leyan. All the chemical reagents were in analytical grade and used without further purification.

1.2 General Characterization

Scanning electron microscopy (SEM) measurements were performed on a JSM-7610F Plus microscope at an acceleration voltage of 10 kV. Transmission electron microscopy (TEM) images were obtained from a JEM-2100F instrument at an acceleration voltage of 120 kV. FT-IR spectra were obtained using Nicolet iN10 MX microscopic infrared spectrometer (Thermo Scientific Co., USA) in the range of 4000 to 400 cm^{-1} under ambient condition. Photoluminescence (PL) spectra of the catalysts were recorded by F-4600 Fluorescence Spectrophotometer with excitation wavelength at 315 nm. Solid-state 13C cross-polarization magic angle spinning NMR (^{13}C-ssNMR) spectra were recorded on a WB 400 MHz Bruker Avance II spectrometer with the contact time of 2 ms (ramp 100) and pulse delay of 4 s. The pore structure of the materials was measured by N_2 adsorption-desorption isotherms at 77 K with Micromeritics ASAP 2460 surface area and porosity analyzer after desolvation at 120 ℃ for 6 h under vacuum. The S_{BET} of the polymers were calculated using the BET model in the ranging of P/P_0 = 0.05–0.30, the total pore volume (V_{total}) of the polymers was calculated from the isotherms at P/P_0 = 0.99 and the pore size distribution (PSD) were all calculated by the non-local density functional theory (NLDFT) method. The X-ray photoelectron spectroscopy (XPS) characterization was detected via Thermo ESCALAB spectrometer with an Al K-α source. The ultraviolet photo-electro spectroscopy (UPS) characterization was detected via Thermo Fisher Nexsa with a He I source. Powder X-Ray Diffraction data were collected over the 2θ range 2-30° on an Advance D8 equipped with Ni-filtered Cu K radiation (40 kV, 100 mA) at room temperature with a scan speed of 2° min^{-1}. The light absorption properties of the catalysts were carried out by solid UV-vis diffuse reflectance spectra (UV-vis DRS, UV-2600, Shimadzu Instrument Co., Ltd.).

1.3 Electrochemical measurements

Electrochemical properties of the COFs materials were measured using a three-electrode system in a chemical workstation with a brand of CHI660E, Chenhua. For the measurements, COFs samples (2 g) were firstly dispersed in 1% Nafion ethanol solution (5 ml) and then ultrasonic 20 min. After that, 100 μL suspension was deposited on the FTO plate to act as the working electrode, while Ag/AgCl electrode worked as the reference electrode and Pt flake acted as the counter electrode. 0.2M Na_2SO_4 aqueous

solution acted as electrolyte during the measurements. Electrochemical impedance spectroscopy (EIS) frequency ranged from 1 Hz to 105 Hz and the photocurrents were measured under visible light irritation with an interval of 30 second, while the Mott-Schottky curves were recorded at 1000 Hz, 1500 Hz and 2000 Hz, respectively. A 0.2 M Na_2SO_4 solution (pH = 2.5) was used as the electrolyte. A 300 W Xenon lamp with a 420 nm cut-off filter was used as the light source during the measurement.

1.4 Photocatalytic H_2O_2 production

The as-synthesized COFs powder photocatalyst (5 mg) was dispersed in a mixed solution containing 40 mL of deionized water. The suspension was well dispersed by ultrasonication and O_2 was bubbled into the suspension for 30 min in the dark. A 300 W Xe lamp (Perfect light, PLS-SXE300) fitted with a 420 nm long-pass filter was used as the light source during the measurement. At given time intervals, the solution filtrated with a 0.22 μm filter to remove the photocatalysts. 0.3 ml of filtered reaction solution was taken and the solution was added into 1 mL potassium hydrogen phthalate ($C_8H_5KO_4$) solution (0.1 M) and 1 mL potassium iodide (KI) solution (0.4 M) and kept for 30 min in dark. H_2O_2 molecules would react with I^- to generate I_3^- , and the amount of I_3^- was measured by a UV spectrophotometer (Shimadzu UV-2460) at its characteristic absorbance peak (350 nm). The standard curve was established by measuring the absorbance of several solutions of H_2O_2 with known concentrations (A=3.363C-0.03872, R^2=0.99965).

For the photocatalytic reaction cycle, after each reaction cycle, the COF powder was recovered by centrifugation and washed with water and ethanol for three times. Afterwards, the sample was dried under vacuum at 120 °C for 12h before next cycling test.

1.5 Detect $\cdot O_2^-$ by NBT

1 mg of COFs (TTB-COF, BQ-TTB-COF and QL-TTB-COF, respectively) and 8 mL of NBT solution (0.05 mM） were mixed and dispersed in a quartz tube. The quartz tube was illuminated by a 300 W xenon lamp (PLS-SXE 300). After irradiation at 30 min, the supernatant was collected by centrifugation, and the UV-Vis spectra were collected.

1.6 Isotope $^{18}O_2$ labeling experiment

Under an $^{18}O_2$ atmosphere, the reaction mixture containing $H_2{}^{16}O$ (2 mL) and TTB-COF or BQ-TTB-COF or QL-TTB-COF (5.0 mg) was exposed to light (300 W xenon lamp (PLS-SXE300)) for 5 h, and then the supernatant was decomposed with MnO_2. The gas phase was analyzed using gas chromatography-mass spectrometry (Shimadzu GC-MS-QP2010 Ultra).

1.7 Isotope $H_2{}^{18}O$ labeling experiment

Under an Ar atmosphere, the reaction mixture containing $H_2{}^{18}O$ (2 mL) and TTD-COF or *io*-TTD-COF or *di*-TTD-COF (5.0 mg) was exposed to light (300 W xenon lamp (PLS-SXE 300)) for 5 h. The gas phase was first analyzed using gas chromatography-mass spectrometry (Shimadzu GC-MS-QP2010 Ultra). The suspension was decomposed with MnO_2, and then the released gas phase was also analyzed

with GC-MS.

1.8 AQY measurements

The apparent quantum yield (AQY) was measured under the illumination of a 300 W Xe lamp with different band-pass filters (λ 0±20 nm) for 1 h. The photocatalyst (10 mg) was added to pure deionized water (40 mL). Ultrasound and O_2 bubbling for half an hour respectively, and the apparent quantum yields were calculated using the following equations:

$$\mathrm{AQY} = \frac{2 \times \text{number of evolved } \mathrm{H_2O_2} \text{ molecules}}{\text{number of incident photons}} \times 100\% = \frac{2 \times \mathrm{CN_A}}{\mathrm{SPt\lambda/hc}} \times 100\%$$

Where C is the H_2O_2 production amount (μmol) per hour; N_A is the Avogadro constant (6.02×10^{23} mol^{-1}); S is the irradiation area (cm^2); P is the monochromatic light intensity (W cm^{-2}) (P is detected by optical power meter); t is the light irradiation time (3600 s); λ is the wavelength of the monochromatic light (nm); h is the Plank constant (6.626×10^{-34} J s); c is the speed of light (3×108 m s^{-1}).

1.9 SCC efficiency measurements

The solar-to-chemical energy conversion (SCC) efficiency was determined by using an AM 1.5 G solar simulator as the light source (300 W Xe lamp). The photocatalytic reaction was carried out in pure deionized water (40 mL) with photocatalysts (10 mg). Ultrasonication and O_2 bubbling for half an hour respectively. During the photocatalytic tests, O_2 was continually bubbled into the bottle. The SCC efficiency was calculated via the following equation:

$$SCC\ efficiency(\%) = \frac{\Delta G_{H_2O_2} \times n_{H_2O_2}}{t_{ir} \times S_{ir} \times I_{AM}} \times 100\%$$

Where $\Delta G_{H_2O_2}$= 117 kJ mol^{-1} is the free energy for H_2O_2 generation (117 kJ mol^{-1}). $n_{H_2O_2}$ is the amount of H_2O_2 generated and tir is the irradiation time (s). The overall irradiation intensity (IAM) of the AM1.5 global spectrum (300-2,500 nm) is 1,000 W m^{-2} and the irradiation areas (Sir) are 4×10^{-4} m^2.

1.10 Rotating disk electrode (RDE) measurements

5 mg of the sample was dispersed in 0.5 mL of ethanol containing 5 μL of Nafion (5 wt%) and sonicated for 10 min. 3-10 μL of the dispersion was then dropped onto a glassy carbon rotating disc electrode and dried at room temperature. In this measurement, the prepared RDE, platinum electrode and Ag/AgCl (saturated KCl) were used as working, counter and reference electrodes, respectively, in 0.1 M phosphate-buffered saline solutions (PBS pH=7) at different rotational speeds (800, 1000, 1200, 1400, 1600 rpm) to obtain the scanning rate at 10 mV s^{-1} linear scanning voltammograms. The average electron transfer numbers (n) were calculated by the Koutecky-Levich equation:

$$\frac{1}{J} = \frac{1}{J_k} + \frac{1}{J_d} \qquad \text{(S1)}$$

$$\frac{1}{J} = \frac{1}{0.62nFC_0D_{O_2}^{2/3}v^{-1/6}\omega^{1/2}} \qquad \text{(S2)}$$

where J is the current density, J_K and J_L are the kinetic and diffusion-limiting current densities, ω is the rotating speed (rpm), n is transferred electron number, F is Faraday constant (96485 C mol^{-1}), C0 is

the bulk concentration of O_2 (1.26×10^{-3} mol cm^{-3}), D_0 is the diffusion coefficient of O_2 ($2.7 \times$10-5 cm^2 s^{-1}), and ν is kinetic viscosity of the electrolyte (0.01 cm^2 s^{-1}).

1.11 In-situ DRIFTS measurement

In situ DRIFTS measurements were performed by an FT-IR spectrometer (Bruker INVENIO S, Germany, MCT detector) using a homemade reaction cell. The samples were placed in the Harrick diffuse reflectance in situ bin. H_2O and O_2 were added to the reactor in the dark. visible light was turned on and each spectrum was collected by averaging 64 scans throughout the reaction.

1.12 DFT Calculations

In this computational study, we first optimized the structures of COFs using the CP2K software package. Subsequently, based on the optimized structures, we performed time-dependent density functional theory (TDDFT) calculations to investigate the charge/hole separation behavior. For the adsorption model calculations, we constructed slab models with periodic boundary conditions applied in the XY directions, while a 15 Å vacuum layer was introduced along the Z direction. The substrate was fixed, and the geometry of the adsorbed molecules was optimized. The adsorption energy was calculated using the formula:

$$E_{ads} = E_{AB} - E_A - E_B$$

The energy of the chemical reaction was determined based on the adsorption energy and the chemical reaction equilibrium, employing the computational hydrogen electrode model, where:

$$U(H^+ + e^-) = \frac{1}{2}U(H_2)$$

All calculations were performed using the generalized gradient approximation (GGA) with the PBE functional, paired with the DZVP-MOLOPT-SR-GTH basis set. The DFT-D3 dispersion correction was applied to account for weak intermolecular interactions. During the calculations, the energy cutoff and real-space cutoff were set to 500 Ry and 50 Ry, respectively. The electrostatic potential was derived from the wavefunction files using Multiwfn, and the results were visualized with VESTA and VMD. Unless otherwise specified, additional analyses were also conducted using Multiwfn.

2. Synthetic Procedures

2.1 Synthesis of TTB-COF[1]

TAPT (35.4 mg, 0.1 mmol), BTPA (39.5 mg, 0.1 mmol), 1,4-dioxane (2.0 ml), mesitylene (2.0 ml), and 6 M aqueous acetic acid (0.2 ml) were added sequentially to the ampoule. After sonication for 15 minutes, the tubes were snap-frozen at 77 K, degassed by a cryopump thawing procedure and sealed with a flame. After heating at 120 ℃ for 72 h, the yellow solid was filtered and washed with THF (10 mL×3). The wet solid was transferred to a Soxhlet extractor and thoroughly washed with THF for 24 h, followed by thorough washing with acetone for 24 h. Finally, the product was evacuated at 25 °C for 12 h and 120 °C for 12 h at 50 mTorr to yield guest-free sample as yellow powder (54.6 mg, 78.8%).

2.2 Synthesis of BQ-TTB-COF[2]

TAPT (35.4 mg, 0.1 mmol), BTPA (39.5 mg, 0.1 mmol) and ammonium iodide (87.1 mg, 0.6 mmol), di-tert-butyl peroxide (112.5 μL, 0.6 mmol), triethylamine (167.5 μL, 0.9 mmol), anhydrous 1,4-dioxane (2.0 mL), mesitylene (2.0 mL) and 6 M aqueous acetic acid (0.2 ml) were added. After sonication for 15 minutes, the tubes were snap-frozen at 77 K, degassed by a cryopump thawing procedure and sealed with a flame. After heating at 120 ℃ for 72 h, the brown solid was filtered and washed with THF (10 mL×3). The wet solid was transferred to a Soxhlet extractor and thoroughly washed with THF for 24 h, followed by thorough washing with acetone for 24 h. Finally, the product was evacuated at 25 °C for 12 h and 120 °C for 12 h at 50 mTorr to yield guest-free sample as brown powder (62.1 mg, 81.1 %).

2.3 Synthesis of QL-TTB-COF[3]

TAPT (35.4 mg, 0.1 mmol), BTPA (39.5 mg, 0.1 mmol) and ammonium iodide (87.1 mg, 0.6 mmol), pyruvic acid (20.8 μL, 0.3 mmol), 2,3-dichloro-5,6-dicyano-1,4-benzoquinone (6.1 mg, 0.27 mmol), anhydrous 1,4-dioxane (2.0 mL), mesitylene (2.0 mL) and 6 M aqueous acetic acid (0.2 ml) were added. After sonication for 15 minutes, the tubes were snap-frozen at 77 K, degassed by a cryopump thawing procedure and sealed with a flame. After heating at 120 ℃ for 72 h, the brown solid was filtered and washed with THF (10 mL×3). The wet solid was transferred to a Soxhlet extractor and thoroughly washed with THF for 24 h, followed by thorough washing with acetone for 24 h. Finally, the product was evacuated at 25 °C for 12 h and 120 °C for 12 h at 50 mTorr to yield guest-free sample as brown powder (76.6 mg, 85.2 %).

3. Supplementary Figures and Tables

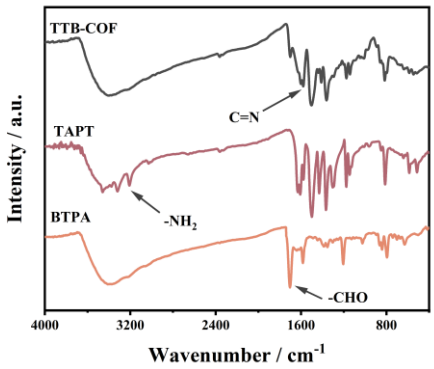

Figure S1. The FT-IR spectra of TTB-COF.

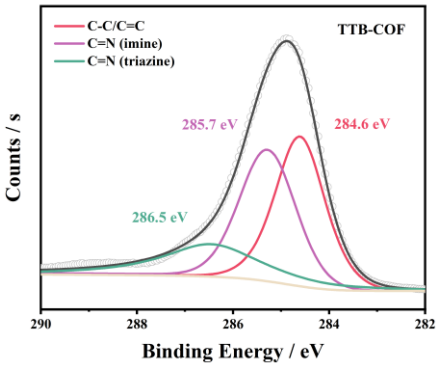

Figure S2. High-resolution XPS spectra of the C 1s of TTB-COF.

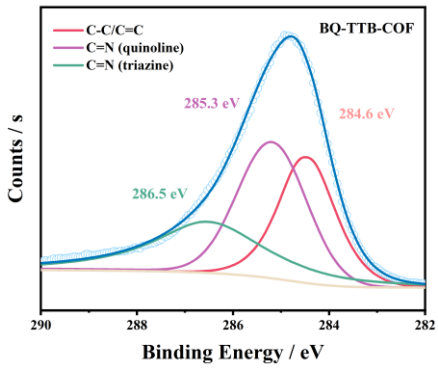

Figure S3. High-resolution XPS spectra of the C 1s of BQ-TTB-COF.

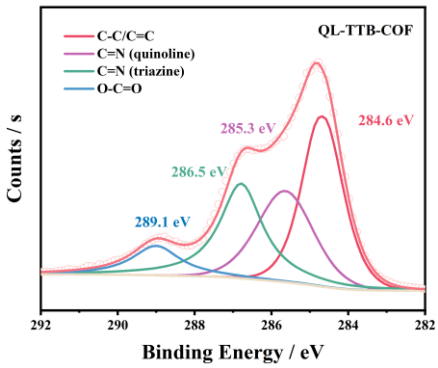

Figure S4. High-resolution XPS spectra of the C 1s of QL-TTB-COF.

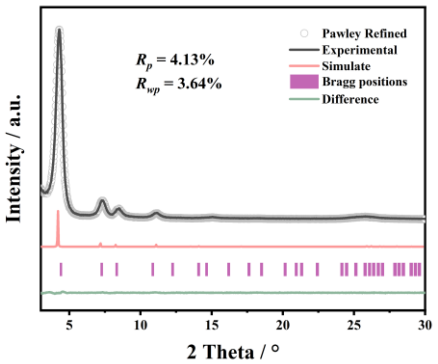

Figure S5. PXRD patterns: the experimental data and simulated patterns for eclipsed AA stacking mode of TTB-COF.

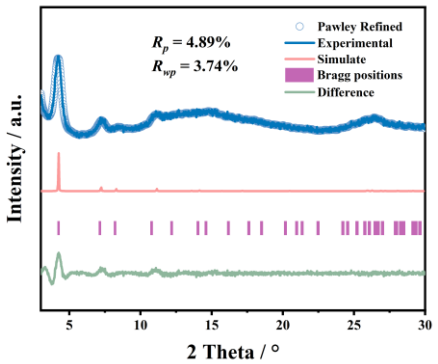

Figure S6. PXRD patterns: the experimental data and simulated patterns for eclipsed AA stacking mode of BQ-TTB-COF.

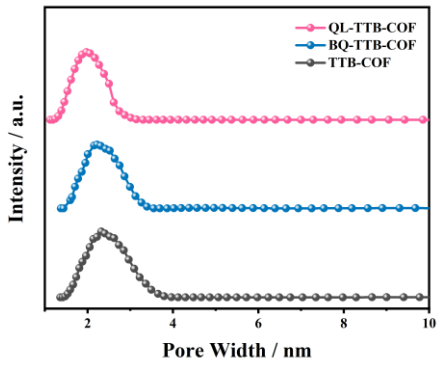

Figure S7. Pore size distribution of TTB-COF, BQ-TTB-COF and QL-TTB-COF.

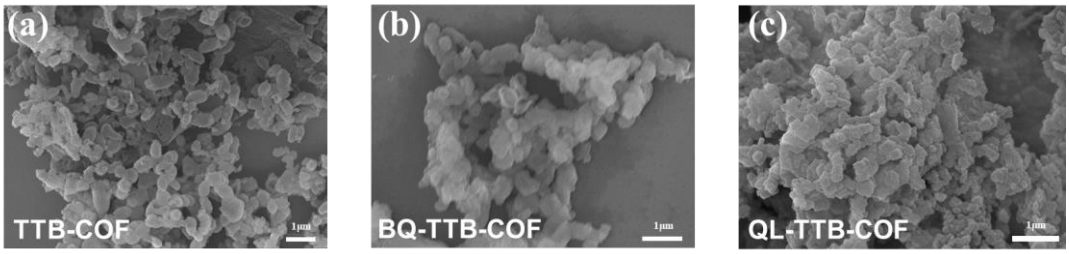

Figure S8. SEM image of (a) TTB-COF, (b) BQ-TTB-COF and (c) QL-TTB-COF.

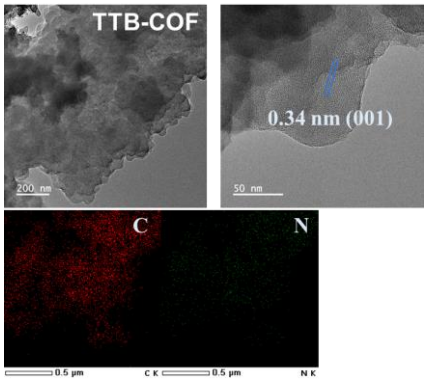

Figure S9. TEM and HR-TEM of TTB-COF.

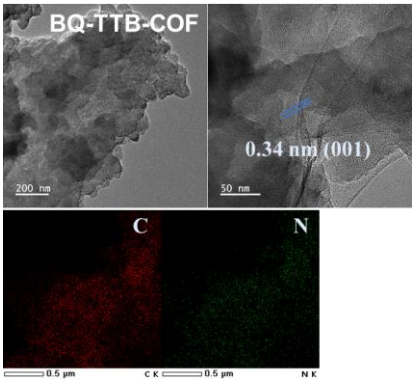

Figure S10. TEM and HR-TEM of BQ-TTB-COF.

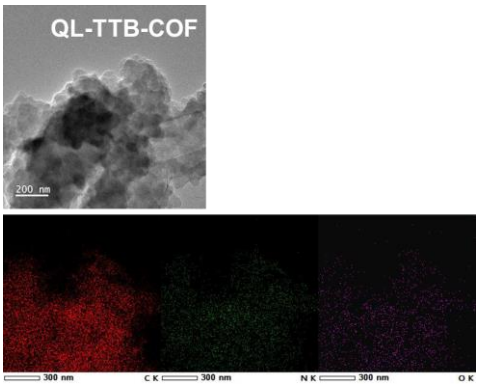

Figure S11. TEM of QL-TTB-COF.

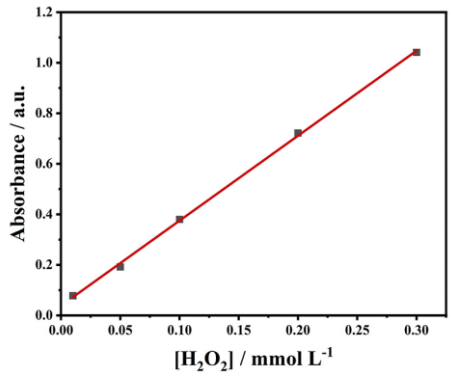

Figure S212. The standard curve for the iodometry method. (A=3.363C-0.03872, R^2=0.99965)

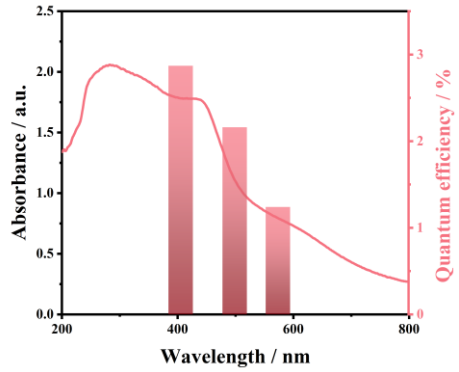

Figure S13. AQYs of QL-TTB-COF at different selected wavelengths (420, 500 and 580 nm).

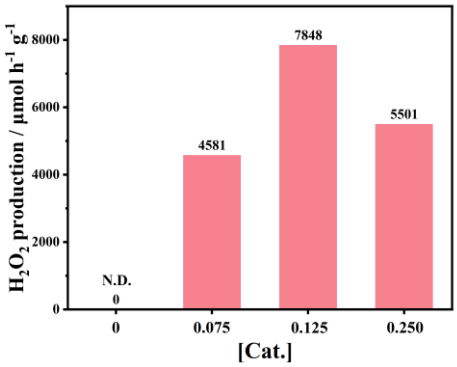

Figure S14. Photocatalytic H_2O_2 production rate of QL-TTB-COF with different concentrations (40 mL

water, λ>420 nm Xe lamp).

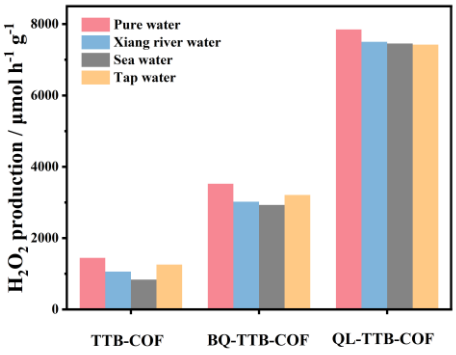

Figure S15. Photocatalytic H_2O_2 production rate of TTB-COF, BQ-TTB-COF and QL-TTB-COF in different kinds of water (5 mg of catalyst in 40 mL water, λ>420 nm Xe lamp).

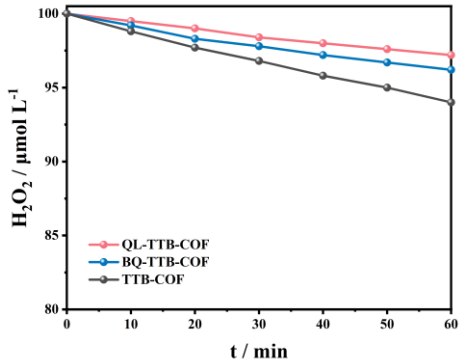

Figure S16. Photocatalytic decomposition of H_2O_2 (C_0=100 μmol L^{-1}) in aqueous solution by TTB-COF, BQ-TTB-COF and QL-TTB-COF. (5 mg of catalyst, λ>420 nm Xe lamp).

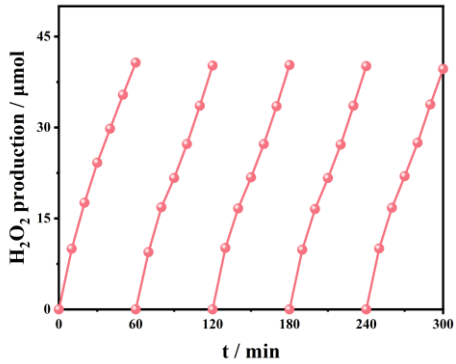

Figure S17. Cycling experiments with QL-TTB -COF (5 mg of catalyst in 40 mL water, λ>420 nm Xe lamp).

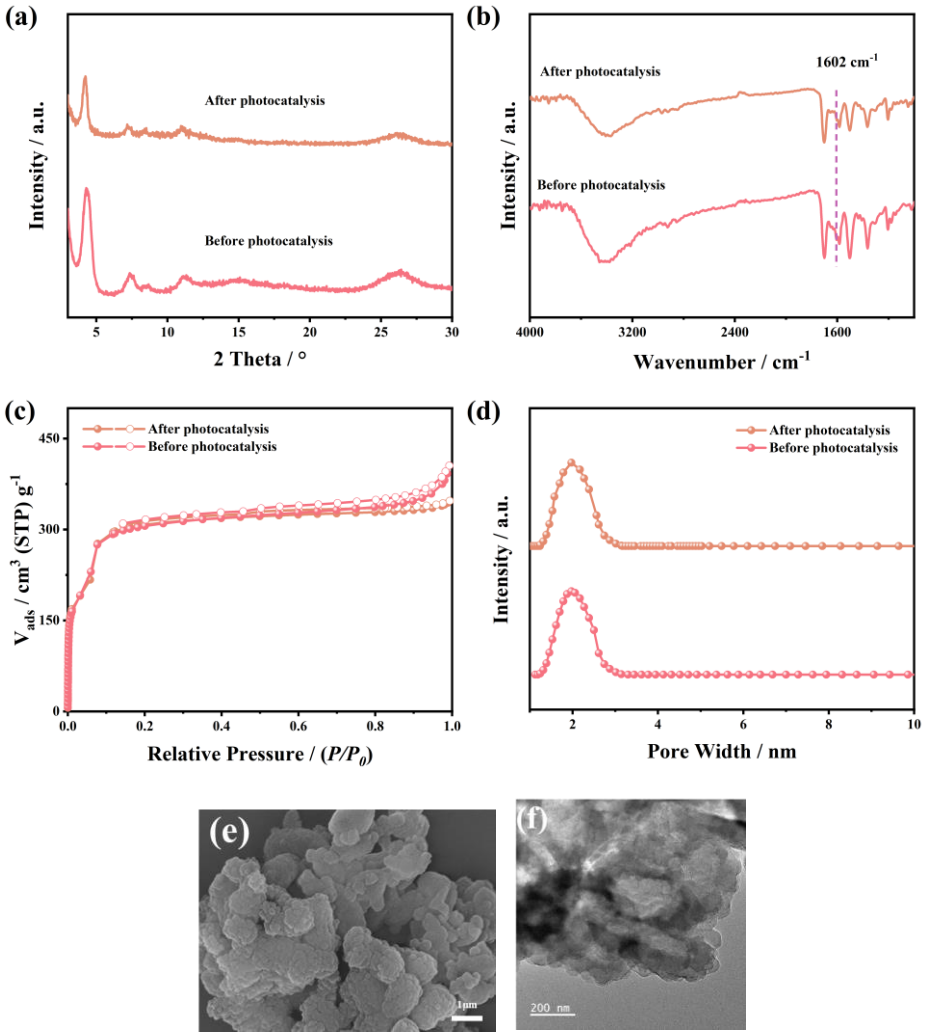

Figure S18. (a) PXRD patterns, (b) FT-IR spectra, (c) N_2 isotherms and (d) pore size distribution of QL-TTB-COF before and after photocatalytic reaction. (e) SEM image and (f) TEM of QL-TTB-COF after photocatalytic reaction.

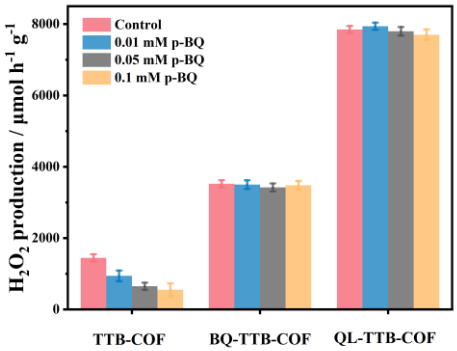

Figure S19. H_2O_2 production of TTB-COF, BQ-TTB-COF and QL-TTB-COF under different p-BQ concentrations. The error bars in the figure represent the standard deviations from triplicate tests.

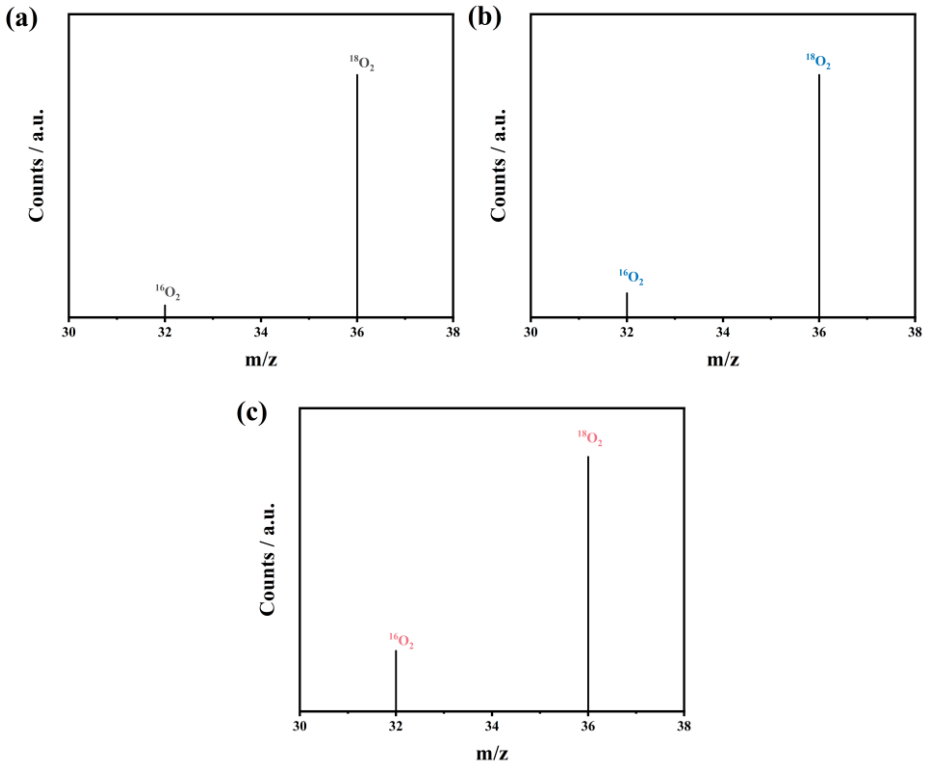

Figure S20. The isotopic experiments with (a) TTB-COF, (b) BQ-TTB-COF and (c) QL-TTB-COF as the photocatalyst in the presence of $H_2{}^{16}O$ and $^{18}O_2$. (1mL sample were taken from the system and injected into the GC-MS spectra for analysis.)

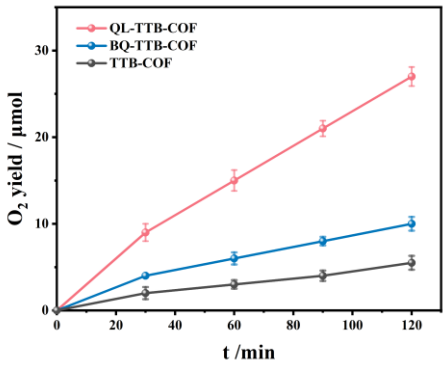

Figure S21. Photocatalytic O_2 evolution by TTB-COF, BQ-TTB-COF and QL-TTB-COF. (Reaction condition: 5 mg catalyst in 40 mL 0.01 M $KBrO_3$, Ar_2, λ>420 nm Xe lamp). Conduct parallel experiments or each, condition three times.

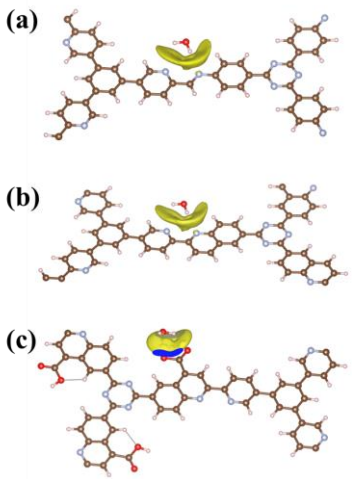

Figure S22. The charge density difference of H_2O molecule on the (a) TTB-COF, (b) BQ-TTB-COF and (c) QL-TTB-COF (isosurface value is 0.001 e $Å^{-3}$).

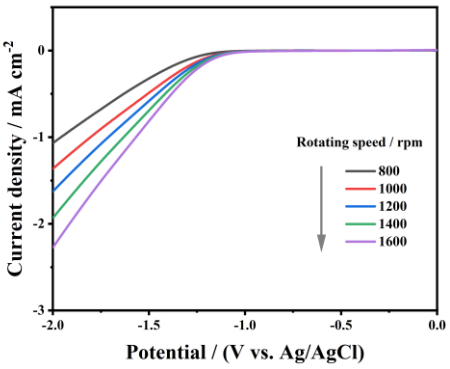

Figure S23. LSV curves using RDE for TTB-COF in rotating speeds from 800 rpm to 1600 rpm.

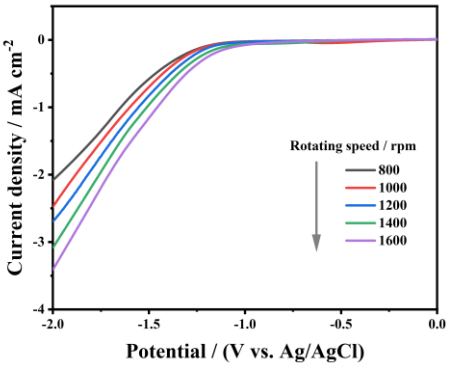

Figure S24 LSV curves using RDE for BQ-TTB-COF in rotating speeds from 800 rpm to 1600 rpm.

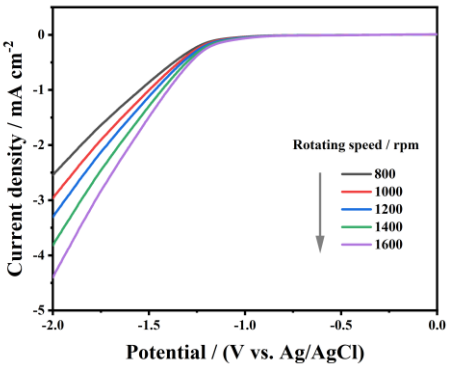

Figure S25. LSV curves using RDE for QL-TTB-COF in rotating speeds from 800 rpm to 1600 rpm.

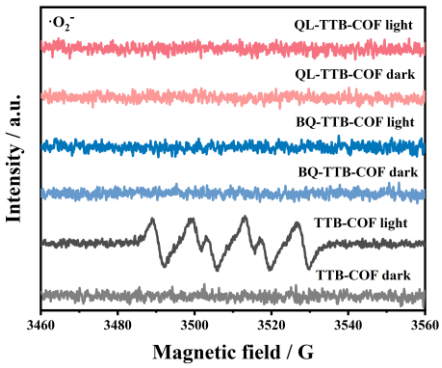

Figure S26. EPR spectra of the photocatalytic system based on the COFs in the dark and after 5-min irradiation of visible light. Conditions: solvent: methanol, spin trapper: DMPO.

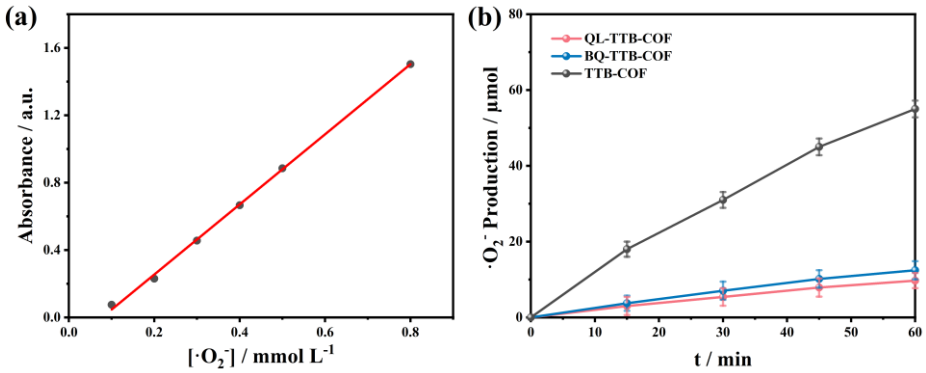

Figure S27. (a) The standard curve for NBT detection of $\cdot O_2^-$ (A=2.081C-0.0616, R^2=0.99918). (b) Time-dependent $\cdot O_2^-$ yield by COFs detected by NBT method.

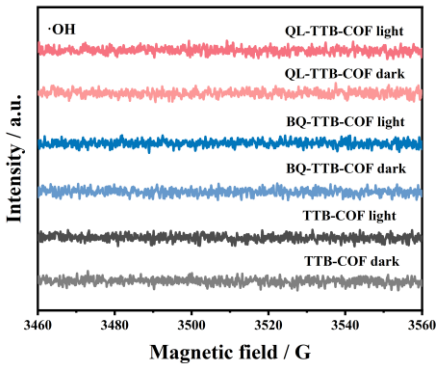

Figure S28. EPR spectra of the photocatalytic system based on COFs in the dark and after 5-min irradiation of visible light.

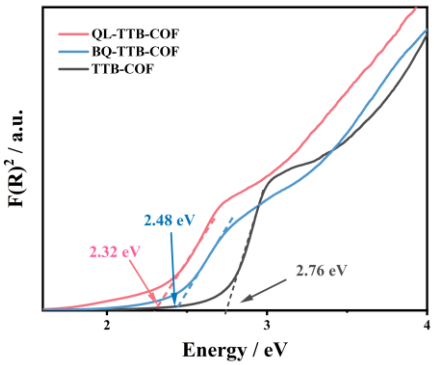

Figure S29. Tauc plot of TTB-COF, BQ-TTB-COF and QL-TTB-COF.

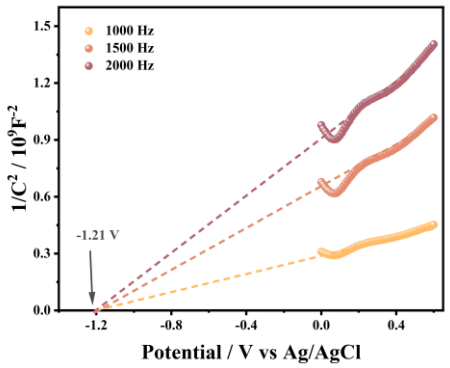

Figure S30. Mott-Schottky plot of TTB-COF.

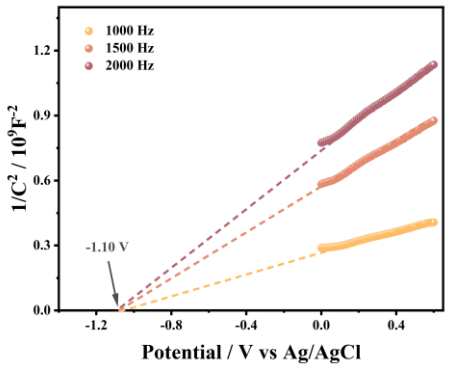

Figure S31. Mott-Schottky plot of BQ-TTB-COF.

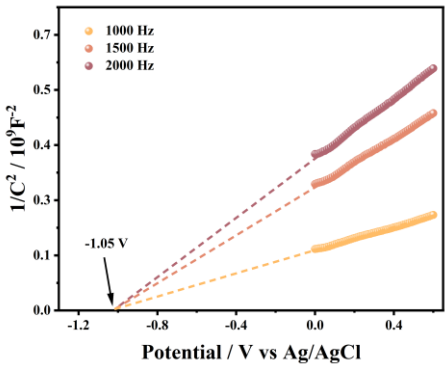

Figure S32. Mott-Schottky plot of QL-TTB-COF.

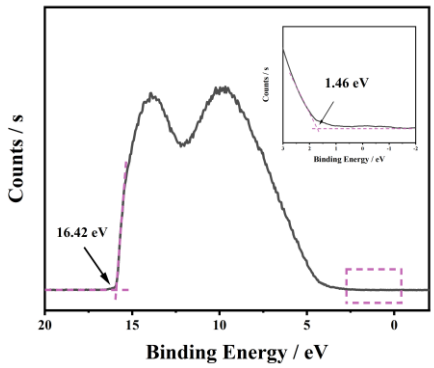

Figure S33. UPS spectra of TTB-COF.

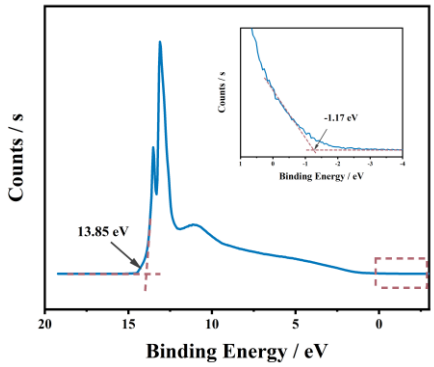

Figure S34. UPS spectra of BQ-TTB-COF.

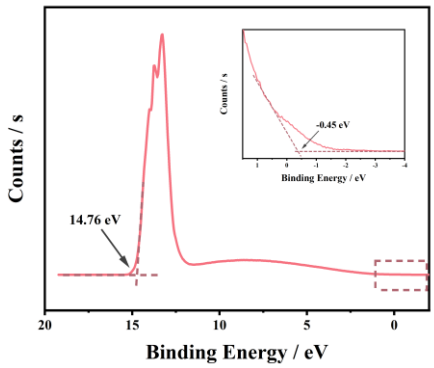

Figure S35. UPS spectra of QL-TTB-COF.

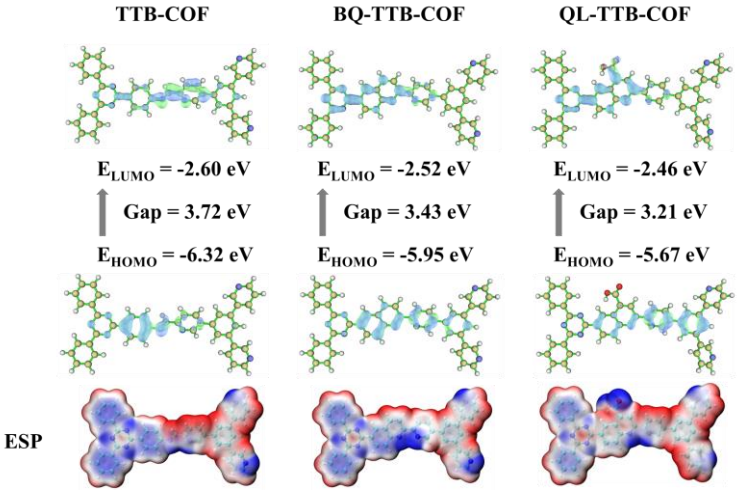

Figure S36. HOMO and LUMO orbital distributions of simplified TTB-COF, BQ-TTB-COF and QL-TTB-COF fragments calculated using density functional theory, along with corresponding electrostatic potential surface (ESP) plots for the TTB-COF, BQ-TTB-COF and QL -TTB-COF models.

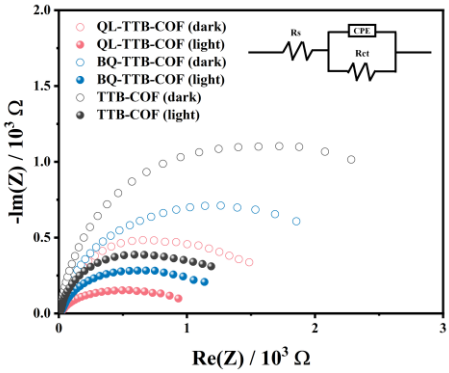

Figure S37. Electrochemical impedance spectroscopy (EIS) Nyquist plots of TTB-COF, BQ-TTB-COF and QL-TTB-COF (under dark and light conditions).

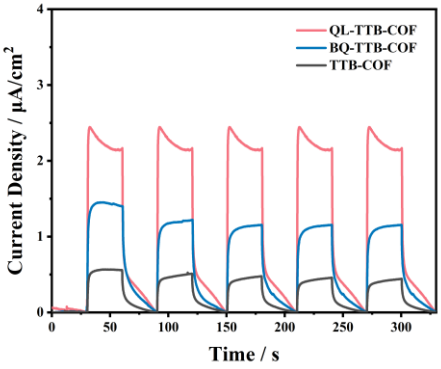

Figure S38. Transient photocurrent responses of TTB-COF, BQ-TTB-COF and QL-TTB-COF.

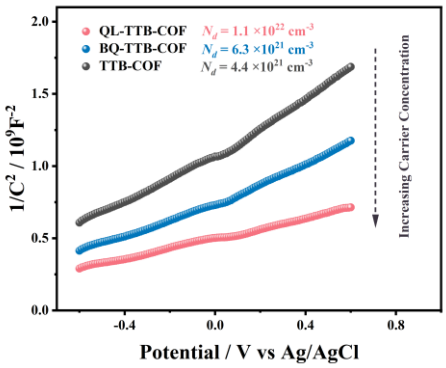

Figure S39. Mott–Schottky plots of COFs under visible light irradiation (λ > 420 nm, 300 W Xe lamp).

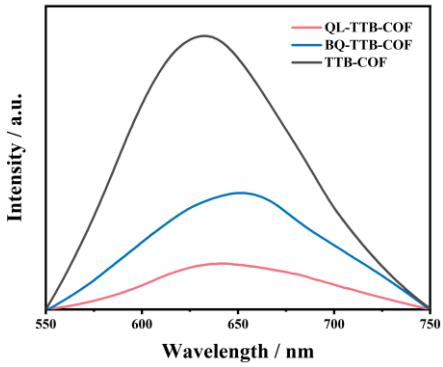

Figure S40. PL spectra of TTB-COF, BQ-TTB-COF and QL-TTB-COF.

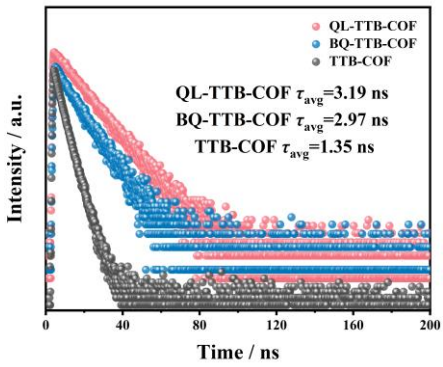

Figure S41. Time-resolved photoluminescence decay plots of TTB-COF, BQ-TTB-COF and QL-TTB-COF.

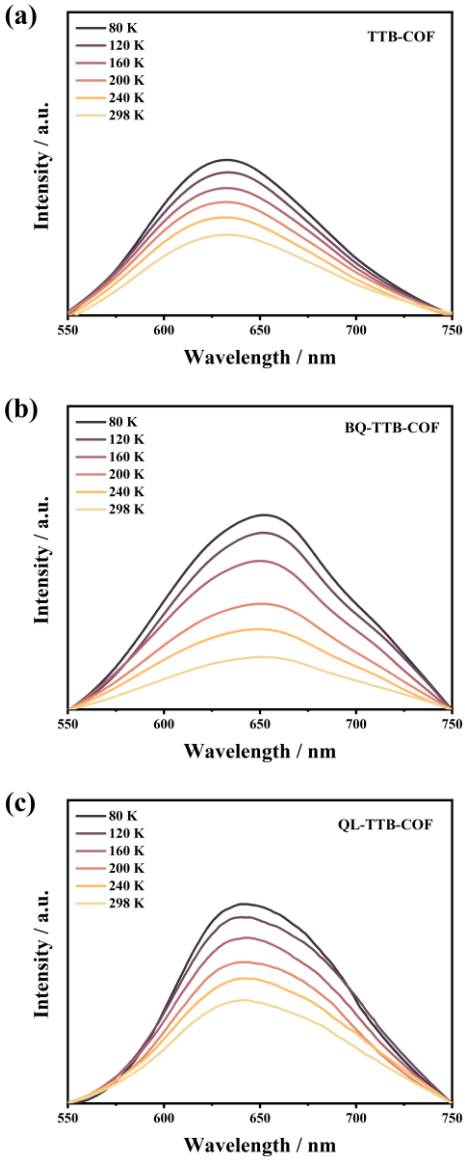

Figure S42. Temperature-dependent photoluminescence spectra of (a) TTB-COF, (b) BQ-TTB-COF and (c) QL-TTB-COF.

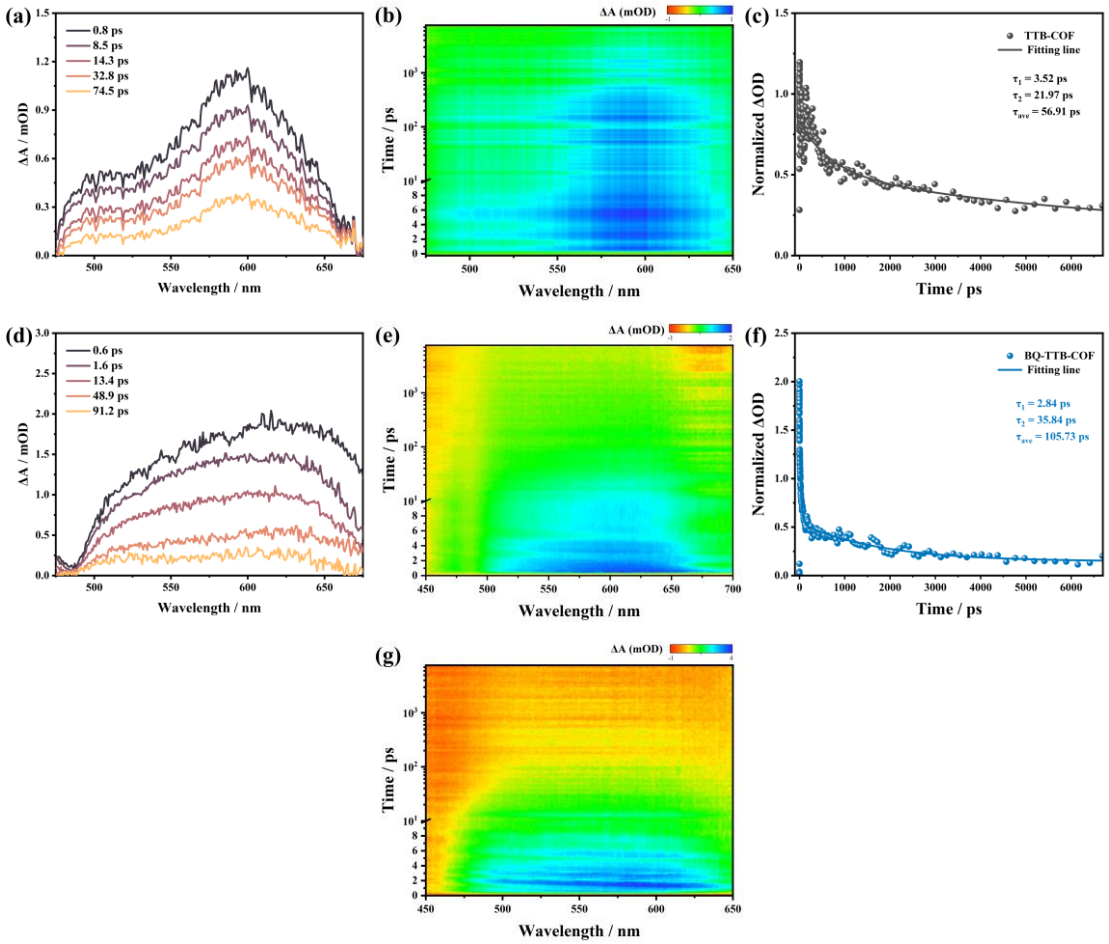

Figure S43. Femtosecond transient absorption spectroscopy (fs-TAS) spectra at different decay time of (a) TTB-COF and (d) BQ-TTB-COF. Pseudo-color images of fs-TAS for (b) TTB-COF, (e) BQ-TTB-COF and (g) QL-TTB-COF, and decay kinetic curves of (c) TTB-COF and (f) BQ-TTB-COF.

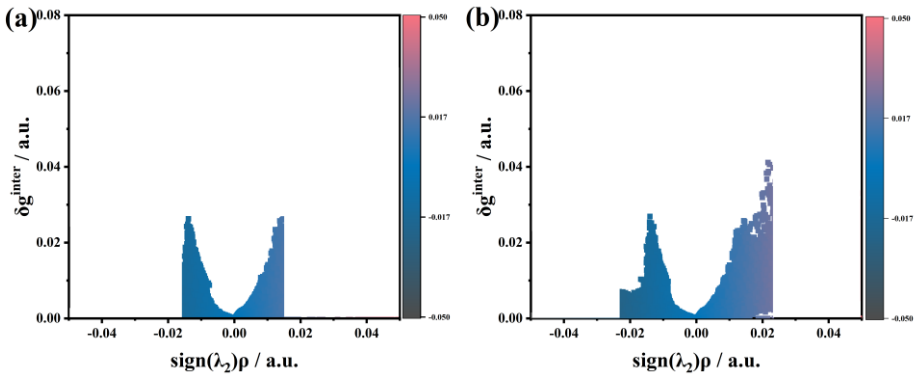

Figure S44. Analysis of the adsorption of H_2O molecules onto (a) TTB-COF and (b) BQ-TTB-COF and the corresponding Independent Gradient Model based on Hirshfeld scatter plots based on the Hirshfeld ligand-based Atom-in-Molecule Topology-Independent Gradient Model.

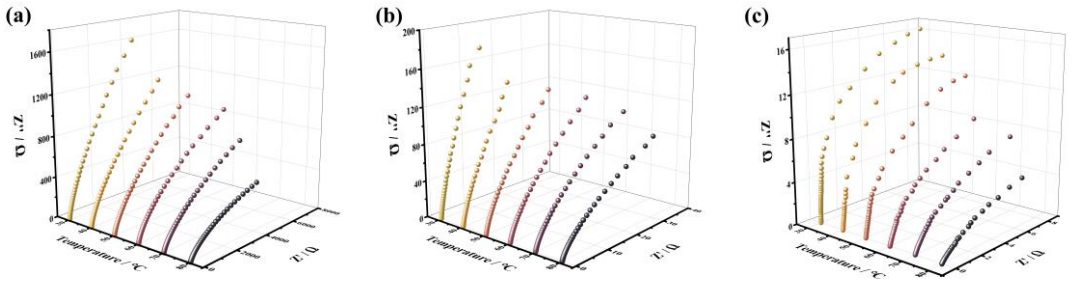

Figure S45. Nyquist plots measured under 98% RH at different temperatures of (a) TTB-COF, (b) BQ-TTB-COF and (c) QL-TTB-COF.

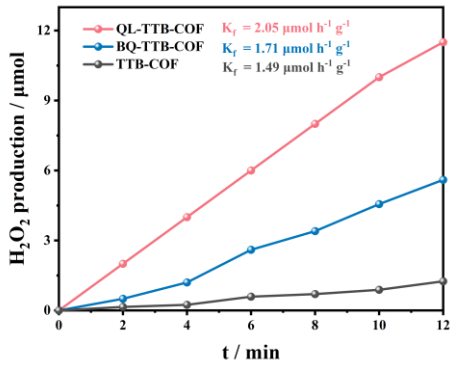

Figure S46. Time-dependent production of H_2O_2 in samples under visible light irradiation during the first 12 minutes

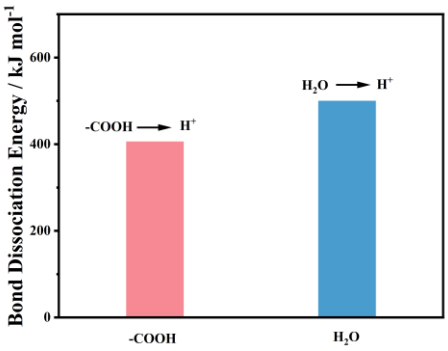

Figure S47. Dissociation energy of the bound proton in -COOH and H_2O.

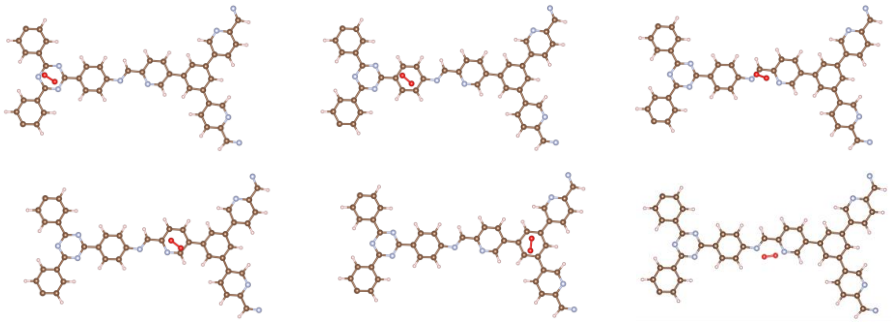

Figure S48. The calculated adsorption energies for O_2 adsorption at different active sites of TTB-COF.

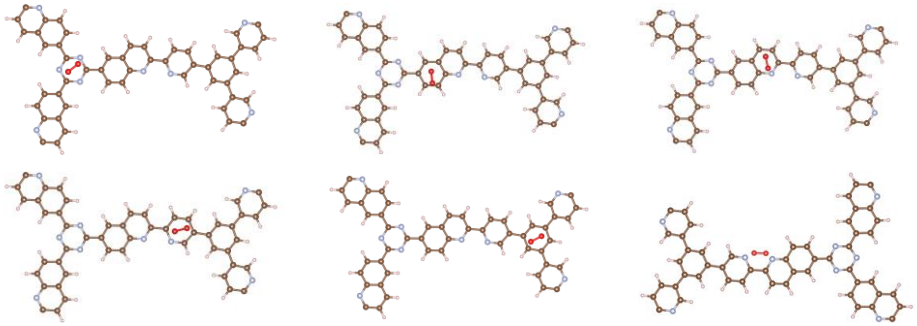

Figure S49. The calculated adsorption energies for O_2 adsorption at different active sites of BQ-TTB-COF.

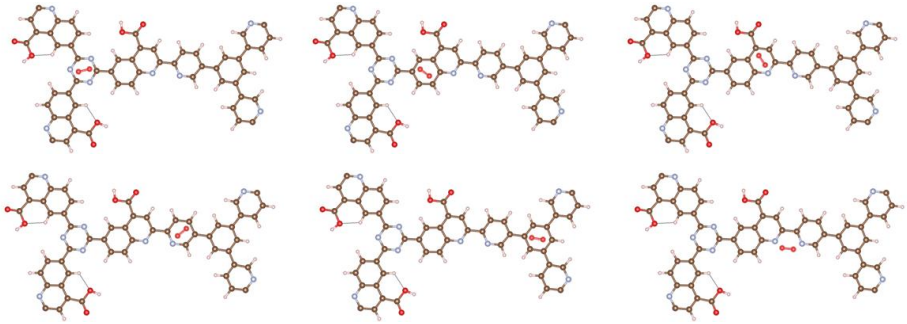

Figure S50. The calculated adsorption energies for O_2 adsorption at different active sites of QL-TTB-COF.

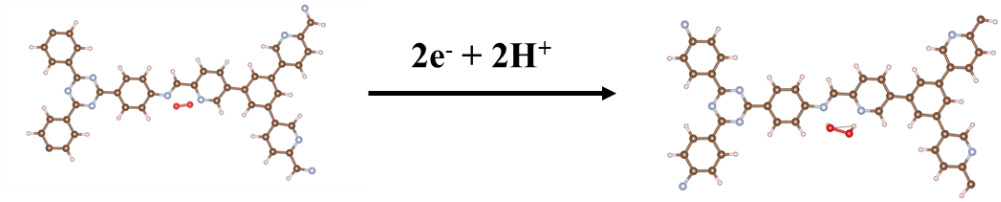

Figure S51. The mechanism of TTB-COF for photocatalytic H_2O_2 formation.

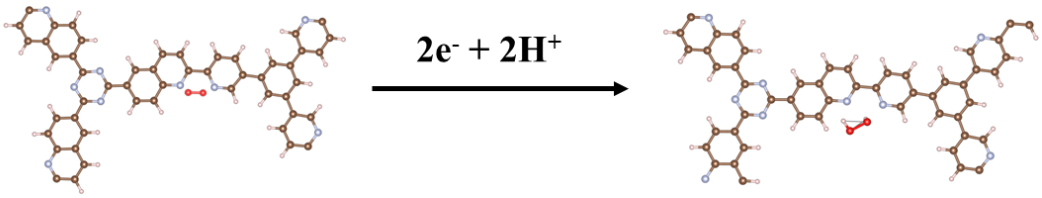

Figure S52. The mechanism of BQ-TTB-COF for photocatalytic H_2O_2 formation.

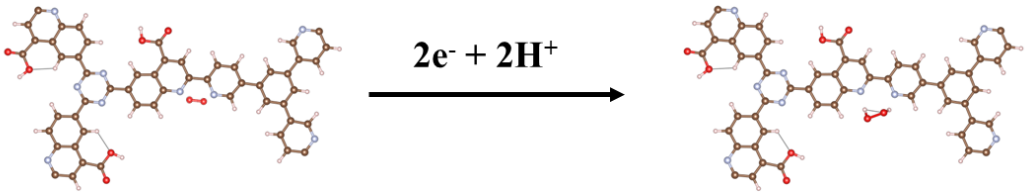

Figure S53. The mechanism of QL-TTB-COF for photocatalytic H_2O_2 formation.

Table S1. Performance of COF-based photocatalysts for overall H_2O_2 photosynthesis.

Photocatalysts	Wavelength / nm	Solvent	[Cat.] / g L^{-1}	H_2O_2 production rate / μmol g^{-1} h^{-1}	AQY at 420 nm/%	
TPDB-NO_2	λ>420	H_2O	0.25	1400	4.36	Appl. Catal. B Environ. 2025, 371, 125263
HITMS-COF-21	λ>420	H_2O (O_2)	0.25	1957	2	ACS Catal. 2025, 15, 5683–5693
Fo-COF	λ>420	H_2O	0.20	2461.8	8.8 (400 nm)	Nano Res., 2026, 19, 94908633
BBT-CAN-1	λ>420	H_2O	0.10	2500	2.7	Adv. Funct. Mater. 2025, 35, 2424035
COF-Thz	λ>420	H_2O	0.05	3701	2.3	Chem. Mater. 2025, 37, 1972–1982
sp^2-COF-CN	λ>420	H_2O	0.25	4469	-	J. Am. Chem. Soc. 2026, 148, 15099-15113
FZU-303	-	H_2O	0.50	4642	7.8	Green Chem., 2026. 28, 7425-7435
COF-BD2	λ>420	H_2O	0.125	5211	14	Angew. Chem. Int. Ed. 2025, 64, e202505621
PTTN-AO COF	λ>420	H_2O	0.10	6024	6.27	Adv. Sci. 2025, 12, 2415194
iTPPy-COF	λ>400	H_2O	0.17	6249	8.3	Angew. Chem. Int. Ed. 2025, 64, e202425617
COF-2CN-2	λ>420	H_2O	0.10	6864	14.13	Angew. Chem. Int. Ed. 2026, e8513334
ivCOF-I	λ>420	H_2O	0.10	6900	15.7	Angew. Chem. Int. Ed. 2026 , e7617241
OPTZ-2-sp2COF	λ>420	H_2O (O_2)	0.16	7613	4.5	ChemSusChem. 2025, 18, 2500624
QL-TTB-COF	**λ>420**	**H_2O**	**0.125**	**7848**	**8.8**	**This Work**
DMAP-BNCOFs	λ>420	H_2O	0.67	8051.4	8.3	J. Am. Chem. Soc. 2025, 147, 24050-24059
DT_2TA-TAPB	λ>420	H_2O	0.20	8587	3.3 (380 nm)	Nat Commun 2025, 16, 5658

Table S2. Contribution of the $2e^-$ ORR pathway and $4e^-$ WOR pathway to photocatalytic H_2O_2 production

Entry	$2e^-$ ORR pathway	$4e^-$ WOR pathway
TTB-COF	98.9%	1.1%
BQ-TTB-COF	96.5%	3.5%
QL-TTB-COF	92.8%	7.2%

Table S3. The EIS simulated resistance values of the reported COFs.

Entry	R_s / kΩ	R_{ct} / kΩ
TTB-COF	55.36	7095
BQ-TTB-COF	47.19	6426
QL-TTB-COF	34.62	5718

Table S4. Electron-hole distribution characterization of the TTB-COF, BQ-TTB-COF and QL-TTB-COF hexagons, derived from Multiwfn.

Entry	Excited transition	S	D (Å)	S/D ($Å^{-1}$)
TTB-COF	$S_0 \rightarrow S_2$	0.54070	1.460	0.36986
BQ-TTB-COF	$S_0 \rightarrow S_2$	0.64573	2.459	0.26260
QL-TTB-COF	$S_0 \rightarrow S_2$	0.43461	2.692	0.16144

References

[1] R. Wang, I. Nath, Jeet Chakraborty, Linyang Wang, P. Van Der Voort. C Decoding chemical structure–interface correlation in covalent organic framework for sustainable organic electrosynthesis. *J. Mater. Chem. A* **2025**, *13*, 36375-36381

[2]. K.-H. Xie, G.-B. Wang, F. Huang, F. Zhao, J.-L. Kan, Z.-Z. Chen, L. Cai, S.-L. Han, Y. Geng, Y.-B. Dong, Multicomponent one-pot construction of benzo[f]quinoline-linked covalent organic frameworks for H_2O_2 photosynthesis. *Nat. Commun.* **2025**, *16*, 3493.

[3]. P. Das, G. Chakraborty, J. Roeser, S. Vogl, J. Rabeah, A. Thomas, Integrating Bifunctionality and Chemical Stability in Covalent Organic Frameworks via One-Pot Multicomponent Reactions for Solar-Driven H_2O_2 Production. *J. Am. Chem. Soc.* **2023**, *145*, 2975–2984.